中国激光

闲频光单谐振 $KTiOAsO_4$ 涡旋光参量振荡器的研究

苏比努尔·牙库甫，周玉霞*，宣闯，冶建强，买里克古丽·艾合买提，焦夏卓，塔西买提·玉苏甫**
新疆师范大学物理与电子工程学院，新疆发光矿物与光功能材料研究重点实验室，新疆 乌鲁木齐 830054

摘要 设计了一种由 1 μm 涡旋光泵浦的闲频光单谐振 $KTiOAsO_4$ 涡旋光参量振荡器，并基于该光参量振荡器在近/中红外波段实现了高光束质量、高能量、窄光谱带宽的涡旋光输出。选取不同曲率半径的输入镜和平面输出镜分别建立平平腔和平凹腔两种腔结构，基于所建结构可以控制泵浦光的轨道角动量（OAM）选择性地传递给输出的信号光或闲频光。当泵浦光最大能量为 20.6 mJ 时，在近红外波段产生了 3.04 mJ 的信号涡旋光（1.535 μm），同时在中红外波段产生了 0.82 mJ 的闲频涡旋光（3.468 μm），它们对应的转换效率分别为 28.21% 和 7.62%。基于泵浦光与谐振闲频光在两种腔型中的空间重叠效率，从理论上解释了泵浦光 OAM 的传递原理。测量得到输出信号光和闲频光的光谱带宽（半峰全宽）分别为 λ_s=0.85 nm 和 λ_i=1.08 nm，其中闲频光在两个正交方向上的光束质量因子分别为 $M_x^2\approx2.1$ 和 $M_y^2\approx2.2$。

关键词 光学器件；涡旋光；闲频光谐振；光参量振荡器；$KTiOAsO_4$
中图分类号 O437 **文献标志码** A **DOI**：10.3788/CJL231009

1 引 言

近年来，具有螺旋形波阵面分布的涡旋光束引起了人们的广泛关注，其光场公式中的方位项因子 $\exp(i\ell\varphi)$（ℓ 表示拓扑荷数，φ 表示方位角）使每个涡旋光子在传播过程中均携带轨道角动量（OAM）$\ell\hbar$[1-2]，从而使其被广泛应用于粒子捕获[3]、光镊[4]、光学微操纵[5]、超分辨率光谱学[6]、量子通信[7]、激光材料加工[8-9]等领域。为了满足上述应用的需求，已经有多种方法被用来产生涡旋光，如利用方位分段螺旋相位板[10]、叉型衍射全息光栅[11]、q-板[12]、空间光调制器[13]、柱透镜模式转换器[14]产生涡旋光以及从激光腔内直接产生涡旋光[15]等。然而，以上方法只能产生波长单一的光波，缺乏波长通用性，极大地限制了涡旋光在其他波长范围内的应用[16]。为了拓展涡旋光的波长，人们提出了多种非线性频率转换技术，例如倍频[17]、和频[18]、光参量振荡[19-21]、光参量放大[22-23]、受激拉曼散射[24]等。特别地，在光参量振荡器中，光与介质之间的非线性相互作用不仅会引起泵浦涡旋光的波长转换，其携带的 OAM 也会同时发生可控性转移。

3～5 μm 波段是典型的“大气红外窗口”，含有大量气体分子的振动吸收峰，在气候检测、痕量气体分析等方面具有巨大潜力[25-26]。该波段的涡旋光在超分辨率显微镜和分子光谱学等领域具有重要的应用价值。为了产生高性能参数的中红外涡旋光，研究人员利用纳秒[27-30]、皮秒[31]、飞秒[32-34]和连续波[35-36]泵浦基于非线性增益介质的光参量振荡器，分别在近红外和中红外波段获得了高能量、高转换效率的涡旋光。本课题组前期基于砷酸钛氧钾（$KTiOAsO_4$，KTA）晶体涡旋光参量振荡器，研究了腔长扩展过程中泵浦光 OAM 的传递原理，结果显示：KTA 晶体特有的光学特性和腔内增益的变化使得谐振腔内的模式相干叠加，进而产生了携带非整数 OAM 的近/中红外涡旋光[37]。从目前的研究现状来看，在近/中红外波段产生涡旋光大多是基于信号光单谐振或双共振的方式，由于未受到腔镜的限制，闲频光会直接输出，从而导致中红外闲频光的光束质量较差。由于闲频光具有更大的光束尺寸和发散角，基于闲频光单谐振的光参量振荡器在谐振时会产生更大的衍射损耗，进而可以有效抑制高阶模的产生，提高闲频光的光束质量，窄化光谱带宽。早在 2005 年，Tiihonen 团队[38]就基于极化的 KTP（磷酸钛氧钾，$KTiOPO_4$）晶体研究了闲频光单谐振光参量振荡器对输出光的影响。他们认为闲频光振荡时会有较大的衍射损耗，这是由于闲频光具有相对较大的发散角，对输出光的光谱和光束质量具有很好的提升作用。山东大学的 Bai 团队[39-40]基于闲频光单谐振的 KTA 光参量振荡器在中红外波段产生了光束质量因子为 1.2 的闲频光，并比较了闲频光单谐振和信号光单谐振两种光参量振荡器对近/中红外输出光光束质量的影响。2019 年，Parsa 等[41]采用闲频光谐振的 MgO∶PPLN（掺

收稿日期：2023-07-11；**修回日期**：2023-08-14；**录用日期**：2023-09-05；**网络首发日期**：2023-09-15
基金项目：国家自然科学基金（12264049，11664041）
通信作者：*zhou_yx0801@sina.com；**taxmamat_84@sina.com

杂氧化镁周期性极化铌酸锂晶体)光纤皮秒光参量振荡器,在中红外波段产生了平均光束质量因子小于1.8的闲频光(4028~2198 nm)。最近,Nandy等[42]通过皮秒光纤泵浦MgO:PPLN闲频光单谐振腔,在1.3~1.5 μm波段得到了光束质量因子小于2.3的激光源。

基于上述实验思路,笔者选择闲频光谐振的涡旋光参量振荡器来探究泵浦涡旋光OAM的传递原理。分别选取平面和凹面两种输入镜搭建平平腔和平凹腔,实现了泵浦涡旋光OAM可控转移给输出的信号光和闲频光,同时得到了高光束质量的中红外涡旋激光源。在泵浦光最大泵浦能量为20.6 mJ时,获得了3.04 mJ的近红外涡旋光和0.82 mJ的中红外涡旋光,对应光的转换效率分别为28.21%和7.62%,中红外涡旋光的光束质量因子分别为$M_x^2\approx2.1$,$M_y^2\approx2.2$。

2 实验设计

由1 μm涡旋光泵浦、闲频光谐振的KTA涡旋光参量振荡器的实验装置如图1所示,其中泵浦源为纳秒调Q Nd:YAG固体激光器(LS-2136LP,脉冲持续时间为25 ns,波长为1.064 μm,脉冲重复频率(PRF)为50 Hz),其输出光束呈高斯模式。使用一个方位分割成16段、相移为$n\pi/8$的螺旋相位板将输出的高斯光束转换成OAM为1的涡旋光束;利用焦距$f=750$ mm的透镜使泵浦光与谐振光之间达到更好的模式匹配。非线性增益介质的光学特性会直接影响光参量振荡器的工作性能。MgO:PPLN相位匹配宽度大,可以实现宽调谐多波长输出,得到了研究人员的青睐,但其输出光束的光谱带宽较宽,光束单色性较差。因此,笔者采用非线性系数大、损伤阈值高、温度敏感性低[43]、输出光束单色性好的KTA晶体作为非线性增益介质。该晶体在x轴($\theta=90°$,$\varphi=0°$)方向被切割,尺寸为5 mm×5 mm×30 mm,满足Ⅱ类非临界相位匹配。为了得到光束质量高、能量高的近/中红外涡旋激光源,笔者选取两种不同参数的输入镜(M1、M2)和平面输出镜(OC)设计了平平腔与平凹腔两种腔型,腔长固定为35 mm。其中:M1采用高透1 μm和高反1.3~5 μm的平面输入镜;M2是曲率半径为500 mm的凹面输入镜,其他参数与M1相同;输出耦合镜OC的参数为对1 μm和1.41~1.54 μm高透,对3.5~4.4 μm波段具有约80%的反射率。基于平平腔和平凹腔两种腔型结构,探究泵浦光OAM在腔内的传递原理,实现泵浦光OAM在三倍波长差下的主动传递。

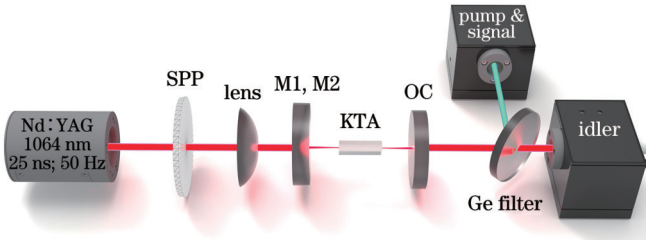

图1 闲频光谐振的KTA涡旋光参量振荡器实验装置图

Fig. 1 Experimental schematic of an idler-resonant optical vortex parametric oscillator based on KTA

3 分析与讨论

利用上述闲频光谐振的涡旋光参量振荡器,分别得到泵浦光、信号光和闲频光的空间分布及自干涉图样,如图2所示。采用传统的CCD相机测量了泵浦光的空间分布和自干涉条纹,如图2(a)、(b)所示。泵浦光的空间强度分布为环形,中心具有相位奇点;泵浦光

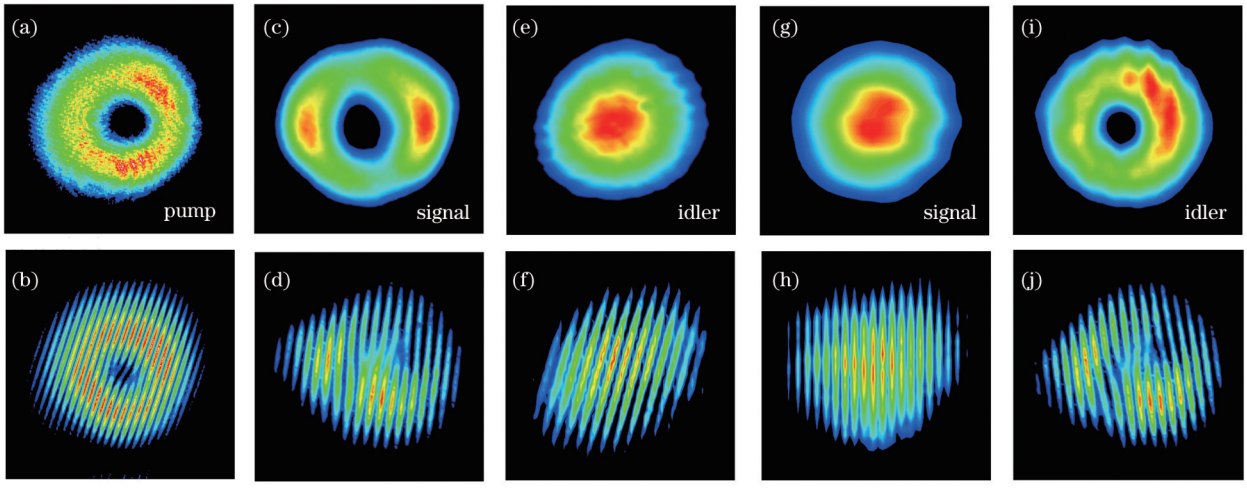

图2 泵浦光、信号光和闲频光的空间分布及自干涉条纹。(a)(b)泵浦光的空间分布和自干涉叉形条纹;采用平平腔时,信号光(c)(d)和(e)(f)闲频光的空间分布和自干涉叉形条纹;采用平凹腔时,信号光(g)(h)和闲频光(i)(j)的空间分布和自干涉条纹

Fig. 2 Spatial forms and interference fringes of pump vortex beam, signal output and idler output. (a)(b) Spatial form and interference fringes of the pump vortex beam; spatial forms and interference fringes of the signal output (c)(d) and idler output (e)(f) for a plane-parallel cavity; spatial forms and interference fringes of the signal output (g)(h) and idler output (i)(j) for a plane-concave cavity

自干涉图样中有一对叉形结构，可以证明泵浦光携带的OAM为1。利用热释电相机（Spiricon Pyrocam III，空间分辨率为75 μm）测量该光参量振荡器产生的近/中红外激光的空间分布和干涉图样。由图2(c)～(f)可以看出：采用平平腔时，输出信号光与泵浦光的空间分布类似，中心具有相位奇点，自干涉图样中有一对叉形条纹，证明信号光携带了泵浦光的OAM；输出闲频光的空间分布呈现为强度由中心向四周逐渐递减的高斯分布，其自干涉条纹是直线形分布，没有叉形条纹，证明闲频光不携带OAM。根据OAM守恒原理，泵浦光的OAM未主动传递给谐振的闲频光输出，而是被动传递给了非谐振的信号光。

为了进一步探究泵浦光OAM的传递规律，选择曲率半径为500 mm的凹面输入镜搭建平凹腔结构，然后在相同的泵浦条件下，通过热释电相机观测输出信号光和闲频光的空间分布和自干涉图样，观测结果如图2(g)～(j)所示。输出信号光的空间分布呈高斯模式分布，自干涉条纹为直线形，没有任何叉形结构（$\ell=0$）；而输出闲频光的空间分布呈环形，与泵浦光的空间分布轮廓一致。从闲频光的自干涉条纹图样中可以看到一对清晰的叉形条纹，证明了在平凹腔中泵浦光的OAM主动传递给中红外闲频光输出，实现了OAM在三倍波长差下的主动传递。为了更进一步确认泵浦光OAM的传递机制，笔者分别采用二阶和三阶涡旋光泵浦该光参量振荡器，结果发现：在平平腔中，输出信号光为携带二阶和三阶OAM的涡旋光，而闲频光呈高斯模式分布；在平凹腔中，输出信号光为高斯光，闲频光分别呈携带二阶和三阶OAM的涡旋模式分布，高阶涡旋泵浦与一阶涡旋泵浦的规律一致。实际上，OAM的传递机制取决于谐振腔内的参数增益，该参数增益由非线性晶体中泵浦光和闲频光的空间重叠效率η决定[27-28]。空间重叠效率η的计算公式为

$$\eta=\frac{4\omega_p^2\omega_i^2}{(\omega_p^2+\omega_i^2)^2},\ \eta\propto\int r\cdot\exp\left(-\frac{r^2}{\omega_p^2}\right)r^{\ell}\cdot\exp\left(-\frac{r^2}{\omega_i^2}\right)r\mathrm{d}r,\tag{1}$$

式中：$\ell=1$为闲频光携带的拓扑荷值；ω_p和ω_i分别为泵浦光和闲频光的光束尺寸。在闲频光单谐振的平平腔中，由于振荡的闲频光具有大的光束尺寸，与泵浦光之间不能有很好的模式重叠，泵浦光的OAM难以传递给谐振闲频光输出；当选择平凹腔时，谐振闲频光的光束尺寸被限制，其尺寸与泵浦光相近，能够实现泵浦光OAM的主动传递。笔者利用LasCAD软件计算了泵浦光尺寸为0.35 mm时平平腔和平凹腔两种腔型中谐振闲频光在晶体中心的光束尺寸，分别为0.73 mm和0.43 mm。同时，笔者通过空间重叠效率公式计算了平平腔和平凹腔中泵浦光与谐振闲频光的空间重叠效率，分别为0.61和0.96。相对于平平腔结构，平凹腔结构中的泵浦光与谐振闲频光空间重叠效率更高，这使得泵浦光的OAM在平平腔下只能被动传递给近红外信号光输出，而在平凹腔中能主动传递给中红外闲频光输出，实现了泵浦光OAM向中红外闲频光的主动传递。

基于闲频光单谐振光参量振荡器对输出光的光谱和光束质量特有的窄化和提升作用[38]，笔者使用高性能扫描单色仪测量了输出信号涡旋光和闲频涡旋光的光谱，测量结果如图3所示。信号光和闲频光对应的波长分别为1.535 μm和3.468 μm，在没有使用任何光谱窄化元件的情况下，信号光和闲频光对应的光谱带宽（半峰全宽，FWHM）分别为λ_s=0.85 nm和λ_i=1.08 nm。相对于信号光单谐振的涡旋光参量振荡器，闲频光单谐振的涡旋光参量振荡器对输出光的光谱确实具有良好的窄化作用。如图4所示，笔者利用刀口

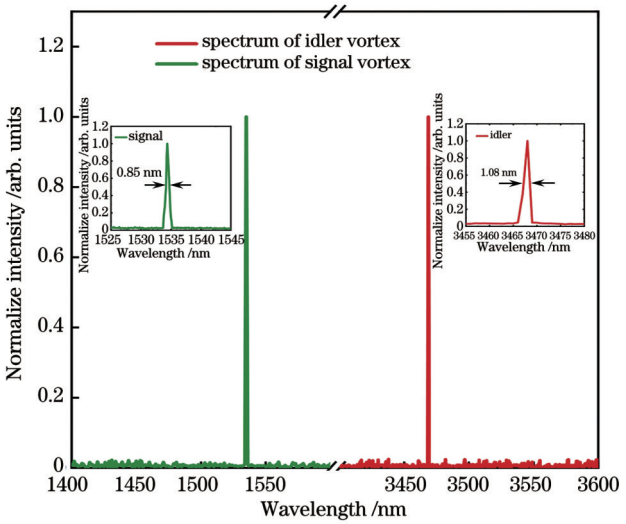

图3 KTA光学参量振荡器中信号光（1.535 μm）和闲频光（3.468 μm）的光谱图，内嵌图给出了信号光和闲频光的光谱带宽

Fig. 3 Spectra of the signal and idler outputs at the wavelength of 1.535 μm and 3.468 μm, respectively. The insets show the spectrum bandwidth of the signal and idler outputs

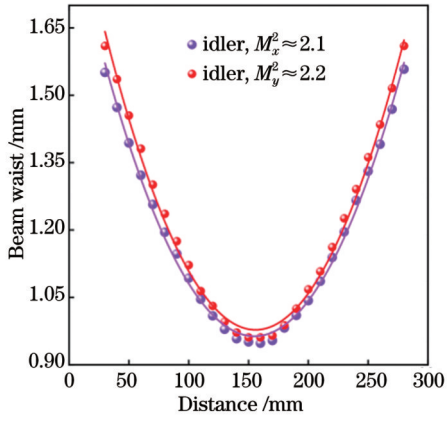

图4 闲频光的光束质量因子（M^2）

Fig. 4 Beam quality factor (M^2) of the idler output

法测得的闲频涡旋光在两个正交方向上的光束质量因子分别为$M_x^2\approx2.1$,$M_y^2\approx2.2$。理想ℓ阶涡旋模的光束质量因子M^2被定义为$2p+|\ell|+1$(p表示径向量子数),对于携带一阶OAM的涡旋光,其理想的光束质量因子为2[44],本文所得闲频光的光束质量接近该理论值。

图5给出了平平腔和平凹腔两种腔结构中输入泵浦光最大能量与输出参量光能量之间的关系。当泵浦光的最大泵浦能量为20.6 mJ时,平平腔输出的信号涡旋光和闲频高斯光的最大能量分别为3.04 mJ和0.74 mJ,对应的转换效率为28.21%和6.93%;平凹腔输出的闲频涡旋光和信号高斯光的最大能量分别为0.82 mJ和3.12 mJ,对应的转换效率为7.62%和29.03%。分析数据可以发现,KTA涡旋光参量振荡器的起振阈值接近10.3 mJ。相对于信号光谐振,闲频光谐振的KTA光参量振荡器的起振阈值更高,而且在振荡过程中,闲频光的损耗也较大。后期可以通过优化腔镜参数、调整谐振腔的设计来进一步提高参量光的转换效率。

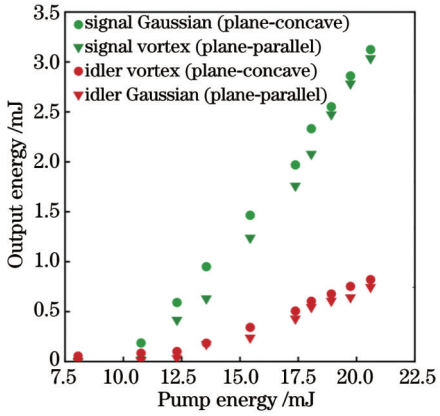

图5 在平平腔和平凹腔两种结构下,泵浦光与输出信号光、闲频光之间的能量关系

Fig. 5 Plot of the output energies of the signal and idler outputs as a function of the pump energy in a plane-parallel cavity and a plane-concave cavity

4 结 论

闲频光谐振的光参量振荡器对输出光的光束质量和光谱具有良好的提升作用。通过1 μm涡旋光泵浦基于KTA晶体的闲频光单谐振涡旋光参量振荡器,同时选取不同参数的输入镜和平面输出镜分别搭建平平腔和平凹腔,使泵浦涡旋光的OAM分别以被动和主动两种方式传递给信号光和闲频光输出,实现了OAM在3倍波长差下的主动转移。在泵浦光最大能量为20.6 mJ时,输出信号涡旋光和闲频涡旋光的最大能量分别为3.04 mJ和0.82 mJ,对应的转换效率分别为28.21%和7.62%。结合闲频光单谐振光参量振荡器的优势,测得中红外闲频光在水平和垂直方向上的光束质量因子分别为$M_x^2\approx2.1$和$M_y^2\approx2.2$,近/中红外涡旋光的光谱带宽(FWHM)分别为$\lambda_s=0.85$ nm和$\lambda_i=1.08$ nm。在实验上实现了高光束质量、高能量近/中红外涡旋光的产生,在理论上解释了泵浦光OAM的传递原理。高光束质量、高能量的中红外涡旋激光源将会大大促进涡旋光在分子光谱和超分辨率显微成像等领域的进一步应用。

参 考 文 献

[1] Allen L, Beijersbergen M W, Spreeuw R J, et al. Orbital angular momentum of light and the transformation of Laguerre-Gaussian laser modes[J]. Physical Review A, 1992, 45(11): 8185-8189.

[2] Yao A M, Padgett M J. Orbital angular momentum: origins, behavior and applications[J]. Advances in Optics and Photonics, 2011, 3(2): 161-204.

[3] Gahagan K T, Swartzlander G A. Optical vortex trapping of particles[J]. Optics Letters, 1996, 21(11): 827-829.

[4] Dholakia K, Čižmár T. Shaping the future of manipulation[J]. Nature Photonics, 2011, 5(6): 335-342.

[5] Toyoda K, Miyamoto K, Aoki N, et al. Using optical vortex to control the chirality of twisted metal nanostructures[J]. Nano Letters, 2012, 12(7): 3645-3649.

[6] Gan Z S, Cao Y Y, Evans R A, et al. Three-dimensional deep sub-diffraction optical beam lithography with 9 nm feature size[J]. Nature Communications, 2013, 4: 2061.

[7] Wang J. Advances in communications using optical vortices[J]. Photonics Research, 2016, 4(5): B14-B28.

[8] Sephton B, Huang Y W, Ambrosio A, et al. Purity and efficiency of hybrid orbital angular momentum-generating metasurfaces[J]. Journal of Nanophotonics, 2020, 14(1): 016005.

[9] Barada D, Juman G, Yoshida I, et al. Constructive spin-orbital angular momentum coupling can twist materials to create spiral structures in optical vortex illumination[J]. Applied Physics Letters, 2016, 108(5): 051108.

[10] Oemrawsingh S S R, van Houwelingen J A W, Eliel E R, et al. Production and characterization of spiral phase plates for optical wavelengths[J]. Applied Optics, 2004, 43(3): 688-694.

[11] Jaiswal V K, Singh R P, Simon R. Producing optical vortices through forked holographic grating: study of polarization[J]. Journal of Modern Optics, 2010, 57(20): 2031-2038.

[12] Karimi E, Piccirillo B, Nagali E, et al. Efficient generation and sorting of orbital angular momentum eigenmodes of light by thermally tuned q-plates[J]. Applied Physics Letters, 2009, 94(23): 231124.

[13] Forbes A, Dudley A, McLaren M. Creation and detection of optical modes with spatial light modulators[J]. Advances in Optics and Photonics, 2016, 8(2): 200-227.

[14] Karimi E. Generation and manipulation of laser beams carrying orbital angular momentum for classical and quantum information applications[EB/OL]. [2023-02-04]. http://www.fedoa.unina.it/3784/.

[15] Ito A, Kozawa Y, Sato S. Generation of hollow scalar and vector beams using a spot-defect mirror[J]. Journal of the Optical Society of America. A, Optics, Image Science, and Vision, 2010, 27(9): 2072-2077.

[16] Omatsu T, Miyamoto K, Lee A J. Wavelength-versatile optical vortex lasers[J]. Journal of Optics, 2017, 19(12): 123002.

[17] Dholakia K, Simpson N B, Padgett M J, et al. Second-harmonic generation and the orbital angular momentum of light[J]. Physical Review A, 1996, 54(5): R3742-R3745.

[18] Li Y, Zhou Z Y, Ding D S, et al. Sum frequency generation with two orbital angular momentum carrying laser beams[J]. Journal of the Optical Society of America B, 2015, 32(3): 407-411.

[19] Martinelli M, Huguenin J A O, Nussenzveig P, et al. Orbital angular momentum exchange in an optical parametric oscillator[J]. Physical Review A, 2004, 70(1): 013812.
[20] Miyamoto K, Miyagi S, Yamada M, et al. Optical vortex pumped mid-infrared optical parametric oscillator[J]. Optics Express, 2011, 19(13): 12220-12226.
[21] Yusufu T, Tokizane Y, Yamada M, et al. Tunable 2-μm optical vortex parametric oscillator[J]. Optics Express, 2012, 20(21): 23666-23675.
[22] Baumgartner R, Byer R. Optical parametric amplification[J]. IEEE Journal of Quantum Electronics, 1979, 15(6): 432-444.
[23] 王海, 赵莉莉, 田俊涛, 等. 基于光参量振荡及放大技术的长波固体激光研究进展[J]. 激光与光电子学进展, 2023, 60(23): 2300007.
Wang H, Zhao L L, Tian J T, et al. Research progress of long-wave solid-state lasers based on optical parametric oscillation and amplification technology[J]. Laser & Optoelectronics Progress, 2023, 60(23): 2300007.
[24] Lee A J, Omatsu T, Pask H M. Direct generation of a first-Stokes vortex laser beam from a self-Raman laser[J]. Optics Express, 2013, 21(10): 12401-12409.
[25] Vainio M, Halonen L. Mid-infrared optical parametric oscillators and frequency combs for molecular spectroscopy[J]. Physical Chemistry Chemical Physics, 2016, 18(6): 4266-4294.
[26] 蔡镐泽, 卜令兵, 龚宇, 等. 3.4 μm 处 NO_2 吸收光谱特性及在差分吸收激光雷达中的应用[J]. 光子学报, 2019, 48(7): 0701001.
Cai G Z, Bu L B, Gong Y, et al. Absorption spectrum characteristics of NO_2 near 3.4 μm and its application in differential absorption lidar[J]. Acta Photonica Sinica, 2019, 48(7): 0701001.
[27] Yusufu T, Niu S J, Tuersun P, et al. Tunable 3 μm optical vortex parametric oscillator[J]. Japanese Journal of Applied Physics, 2018, 57(12): 122701.
[28] Niu S J, Wang S T, Ababaike M, et al. Tunable near- and mid-infrared (1.36–1.63 μm and 3.07–4.81 μm) optical vortex laser source[J]. Laser Physics Letters, 2020, 17(4): 045402.
[29] Ababaike M, Wang S T, Aierken P, et al. Near and mid-infrared optical vortex parametric oscillator based on KTA[J]. Scientific Reports, 2021, 11: 8013.
[30] 孟君, 丛振华, 赵智刚, 等. 百赫兹大能量KTA双波长光参量振荡器[J]. 中国激光, 2021, 48(12): 1201009.
Meng J, Cong Z H, Zhao Z G, et al. 100 Hz high-energy KTA dual-wavelength optical parametric oscillator[J]. Chinese Journal of Lasers, 2021, 48(12): 1201009.
[31] Sharma V, Kumar S C, Samanta G K, et al. Tunable, high-power, high-order optical vortex beam generation in the mid-infrared[J]. Optics Express, 2022, 30(2): 1195-1204.
[32] Camper A, Park H, Lai Y H, et al. Tunable mid-infrared source of light carrying orbital angular momentum in the femtosecond regime[J]. Optics Letters, 2017, 42(19): 3769-3772.
[33] Tong H, Xie G Q, Qiao Z, et al. Generation of a mid-infrared femtosecond vortex beam from an optical parametric oscillator[J]. Optics Letters, 2020, 45(4): 989-992.
[34] 衡家兴, 冯玺, 刘沛, 等. 飞秒光学参量振荡器的腔内光谱展宽技术研究进展[J]. 中国激光, 2022, 49(12): 1201004.
Heng J X, Feng X, Liu P, et al. Research progress of intracavity spectrum broadening technology of femtosecond optical parametric oscillator[J]. Chinese Journal of Lasers, 2022, 49(12): 1201004.
[35] Aadhi A, Sharma V, Singh R P, et al. Continuous-wave, singly resonant parametric oscillator-based mid-infrared optical vortex source[J]. Optics Letters, 2017, 42(18): 3674-3677.
[36] 王海龙, 杨慧琦, 苏静, 等. 基于单共振光学参量振荡器实现近红外到中红外激光输出的实验研究[J]. 中国激光, 2022, 49(18): 1801005.
Wang H L, Yang H Q, Su J, et al. Experimental study of near-infrared to mid-infrared laser output based on single resonant optical parametric oscillator[J]. Chinese Journal of Lasers, 2022, 49(18): 1801005.
[37] Zhou Y X, Yusufu T, Ma Y Y, et al. Generation of tunable, non-integer OAM states from an optical parametric oscillator[J]. Applied Physics Letters, 2023, 122(12): 121106.
[38] Tiihonen M, Pasiskevicius V, Laurell F. Spectral and spatial limiting in an idler-resonant PPKTP optical parametric oscillator [J]. Optics Communications, 2005, 250(1/2/3): 207-211.
[39] Bai F, Wang Q P, Liu Z J, et al. Idler-resonant optical parametric oscillator based on $KTiOAsO_4$[J]. Applied Physics B, 2013, 112 (1): 83-87.
[40] Bai F, Wang Q P, Liu Z J, et al. Comparison of signal-resonant and idler-resonant KTA-SROs[J]. Chinese Optics Letters, 2016, 14(7): 071402.
[41] Parsa S, Kumar S C, Nandy B, et al. Yb-fiber-pumped, high-beam-quality, idler-resonant mid-infrared picosecond optical parametric oscillator[J]. Optics Express, 2019, 27(18): 25436-25444.
[42] Nandy B, Kumar S C, Ebrahim-Zadeh M. Yb-fiber-pumped high-average-power picosecond optical parametric oscillator tunable across 1.3–1.5 μm[J]. Optics Express, 2022, 30(10): 16340-16350.
[43] 卞进田, 孔辉, 徐海萍, 等. 3.5 μm $KTiOAsO_4$ 光参量振荡器温度调谐特性[J]. 中国激光, 2021, 48(4): 0401015.
Bian J T, Kong H, Xu H P, et al. Temperature tuning properties of 3.5- μm $KTiOAsO_4$ optical parametric oscillator[J]. Chinese Journal of Lasers, 2021, 48(4): 0401015.
[44] Ramee S, Simon R. Effect of holes and vortices on beam quality [J]. Journal of the Optical Society of America A, 2000, 17(1): 84-94.

Idler-Resonant Optical Vortex Parametric Oscillator Based on $KTiOAsO_4$

Subinuer Yakufu, Zhou Yuxia*, Xuan Chuang, Ye Jianqiang, Mailikeguli Aihemaiti, Jiao Xiazhuo, Taximaiti Yusufu**

Xinjiang Key Laboratory for Luminescence Minerals and Optical Functional Materials, School of Physics and Electrical Engineering, Xinjiang Normal Unibersity, Urumqi 830054, *Xinjiang, China*

Abstract

Objective Optical vortex lasers, with good beam quality in the mid-infrared spectral region, has many interesting applications such as super-resolution molecular absorption microscopy and molecular spectroscopy. The optical parametric oscillator (OPO) has been established as the most direct method to change the wavelength and transition the orbital angular momentum (OAM) of an optical vortex pump beam. A single-idler resonant cavity can produce a high-quality mid-infrared vortex output. However, one of the main challenges has been to manage the transfer of OAM from the pump beam to the mid-infrared idler output, especially given the

significant wavelength difference—over three times—between the 1 μm pump and 3.5 μm idler beam. This discrepancy complicates achieving high spatial overlap efficiency between the pump and idler vortex modes in the optical vortex pumped idler-resonant parametric oscillator. By choosing cavity mirrors with the correct radius of curvature, a half-symmetric OPO system can facilitate the transfer of the pump beam's OAM to the idler output, ultimately producing a high-quality mid-infrared vortex beam.

Methods In the paper, the idler single resonant optical vortex parametric oscillator based on KTA was examined. A conventional flash-lamped *Q*-switched Nd∶YAG laser (with a Gaussian spatial form, pulse duration of 25 ns, wavelength of 1.064 μm, and pulse repetition frequency of 50 Hz) was employed as the pump source. The laser output was converted into a first-order optical vortex beam using a spiral phase plate. This beam was then focused into a non-critically phase-matched KTA crystal with dimension of 5 mm×5 mm×30 mm. A plane-parallel cavity was formed using M1, which had high transmission for the pump and high reflection for the idler output beam, and an OC that had high transmission for the pump and signal beams, and a partial reflectivity (80%) for the 3.5 μm (idler) beam. A plane-concave cavity was created using a plane-concave M2 (with a curvature radius of 500 mm) that was anti-reflection coated for the pump field and high-reflection coated for the idler beam. An OC, which was partially reflective (R=80%) for the idler field and high-transmitting for the pump and signal fields, was used. The pump beam was observed using a conventional CCD camera. The spatial forms and wavefronts of the signal and idler outputs were measured with a pyroelectric camera (Spiricon Pyrocam III; with a spatial resolution of 75 μm). A lateral shear interferometer with a Mach-Zehnder geometry was used, allowing the optical vortex output to interfere with its own copy, given a proper lateral displacement.

Results and Discussions By using an input mirror with an appropriate radius of curvature and a flat output mirror, plane-parallel and plane-concave cavities are established, respectively. This setup enables the selective transfer of the pump beam's orbital angular momentum to either the signal or idler outputs. The plane-concave cavity produces a high-quality mid-infrared vortex beam with M^2 factors of 2.1 and 2.2 in the two orthogonal directions, as shown in Fig. 4. We achieve 0.82 mJ of 3.468 μm mid-infrared vortex output and 3.04 mJ of 1.535 μm near-infrared vortex output, with a maximum pump energy of 20.6 mJ. This corresponds to slope efficiencies of 28.21% and 7.62%, as depicted in Fig. 5. The transfer principle of OAM is theoretically elucidated by considering the spatial overlap efficiency between pump and idler fields in the two cavities. The spectral bandwidths (FWHM) of the signal and idler outputs are measured as $\Delta\lambda_s$=0.85 nm and $\Delta\lambda_i$=1.08 nm (Fig. 3), respectively.

Conclusions To produce high beam quality and high energy vortex laser in the near/mid-infrared band, an idler-resonant mid-infrared optical vortex parametric oscillator, formed by a 1 μm optical vortex pumped KTA, is constructed. We obtain 0.82 mJ of 3.468 μm mid-infrared vortex output and 3.04 mJ of 1.535 μm near-infrared vortex output at the maximum pump energy of 20.6 mJ, corresponding to a slope efficiency of 28.21% and 7.62%, respectively. With appropriate radius curvature of the cavity mirrors, the plane-concave OPO system enables the OAM of the pump beam transfer to the idler output, and it delivers high beam quality mid-infrared vortex beam. Combined with the advantages of the idler single resonant optical vortex parametric oscillator, the beam quality factors of mid-infrared idler beam in the horizontal and vertical directions are $M_x^2\approx2.1$ and $M_y^2\approx2.2$, respectively, and the spectral bandwidths of near/mid-infrared vortex are $\Delta\lambda_s$=0.85 nm and $\Delta\lambda_i$=1.08 nm, respectively.

Key words optical devices; optical vortex; idler-resonant; optical parametric oscillator; $KTiOAsO_4$